2011

Combined optical and acoustical method for determination of thickness and porosity of transparent organic layers below the ultra-thin film limit

Keith B. Rodenhausen Jr.
University of Nebraska-Lincoln, kbrod@engr.unl.edu

Tadas Kasputis
University of Nebraska-Lincoln, s-tkasput1@unl.edu

Angela K. Pannier
University of Nebraska - Lincoln, apannier2@unl.edu

J. Y. Gerasimov
University of Nebraska-Lincoln

R. Y. Lai
University of Nebraska-Lincoln, rlai2@unl.edu

See next page for additional authors

Combined optical and acoustical method for determination of thickness and porosity of transparent organic layers below the ultra-thin film limit

K. B. Rodenhausen,[1,a)] T. Kasputis,[2,3] A. K. Pannier,[2] J. Y. Gerasimov,[4] R. Y. Lai,[4] M. Solinsky,[5] T. E. Tiwald,[6] H. Wang,[7] A. Sarkar,[7] T. Hofmann,[7] N. Ianno,[7] and M. Schubert[7]

[1]*Department of Chemical and Biomolecular Engineering, University of Nebraska-Lincoln, Lincoln, Nebraska 68588, USA*
[2]*Department of Biological Systems Engineering, University of Nebraska-Lincoln, Lincoln, Nebraska 68588, USA*
[3]*Biomedical Engineering Program, University of Nebraska-Lincoln, Lincoln, Nebraska 68588, USA*
[4]*Department of Chemistry, University of Nebraska-Lincoln, Lincoln, Nebraska 68588, USA*
[5]*The Procter & Gamble Company, 11810 E. Miami River Rd., Cincinnati, Ohio 45252, USA*
[6]*J. A. Woollam Co., Inc., 645 Main Street, Suite 102, Lincoln, Nebraska 68508, USA*
[7]*Department of Electrical Engineering, University of Nebraska-Lincoln, Lincoln, Nebraska 68588, USA*

(Received 24 May 2011; accepted 2 October 2011; published online 28 October 2011)

Analysis techniques are needed to determine the quantity and structure of materials composing an organic layer that is below an ultra-thin film limit and in a liquid environment. Neither optical nor acoustical techniques can independently distinguish between thickness and porosity of ultra-thin films due to parameter correlation. A combined optical and acoustical approach yields sufficient information to determine both thickness and porosity. We describe application of the combinatorial approach to measure single or multiple organic layers when the total layer thickness is small compared to the wavelength of the probing light. The instrumental setup allows for simultaneous *in situ* spectroscopic ellipsometry and quartz crystal microbalance dynamic measurements, and it is combined with a multiple-inlet fluid control system for different liquid solutions to be introduced during experiments. A virtual separation approach is implemented into our analysis scheme, differentiated by whether or not the organic adsorbate and liquid ambient densities are equal. The analysis scheme requires that the film be assumed transparent and rigid (non-viscoelastic). We present and discuss applications of our approach to studies of organic surfactant adsorption, self-assembled monolayer chemisorption, and multiple-layer target DNA sensor preparation and performance testing. [doi:10.1063/1.3653880]

I. INTRODUCTION

Organic layers of few-nm thickness are important for chemical and biological detection,[1] tissue scaffolding,[2] detergent,[3] and surface property tuning[4] applications. Both qualitative and quantitative understanding of organic adsorbate attachment to solid surfaces is of high contemporary interest, especially if performed within liquid ambient. Porosity is a measure of the solvent content of the layer and may be used in further analysis of surface coverage and structural conformation of the organic layer. Measurement of the porosity of an organic layer in a liquid environment is a challenge, particularly if the physical thickness of the layer is on the order of a few nm. *In situ* instrumentation and analysis methods are needed to effectively monitor organic layers as they attach, detach, or change conformational structure in their liquid environments. Optical and acoustical methods, such as spectroscopic ellipsometry and piezoelectric surface resonance techniques, are widely employed for non-invasive, contactless, *in situ* monitoring of organic layer formation. However, for ultra-thin organic layers, neither optical nor acoustical techniques can separate between porosity and thickness independently. The ultra-thin film limit is reached when the total thickness of the organic layer is less than a certain, small fraction of the probing wavelength. At such small thickness, the organic layer may be considered rigid because it does not reveal sufficient viscoelasticity upon measurement. As discussed in further detail below, the ultra-thin film limit is reached when $2\pi nd/\lambda \ll 1$, where d is the thickness of the organic layer, n its index of refraction, and λ is the wavelength of probing light in a linear polarization-dependent optical experiment. For an experiment performed in the visible/near-infrared spectrum (350–1000 nm), the ultra-thin film limit is on the order of a few nm. Acquiring quantitative porosity information from an experiment can be useful for constructing model scenarios that provide insight into the physical structure of the thin film. Thus, (a) instrumentation sensitive to nm-scale organic film growth with sufficient time resolution to allow dynamic measurements (each a series of data sets taken at regular intervals, or "time slices" of data) and (b) analysis methods capable of yielding the dynamic thickness and porosity of an organic ultra-thin film are particularly advantageous.

Porosity can be defined by a mass or volume fraction. In this work, we describe porosity in the form of mass and volume adsorbate fraction parameters f_o^m and f_o^V, respectively, which are bound between zero and unity. The porosity of organic thin films affects material properties due to the absence of adsorbate and the contribution of ambient inclusions. We

a)Electronic mail: kbrod@cox.net.

consider a porous organic thin film to be completely homogenous or to have a homogenous and random distribution of locally heterogeneous inclusions such that the thin film can be considered isotropic on a scale of, or much larger than, the probing wavelength.

Previous experimental efforts to study the porosity of organic ultra-thin films remained qualitative [5–8] or obtained the film thickness and porosity using additional *ex situ*[9] or separate *in situ* measurement instrumentation.[10] Stålgren, Erikkson, and Boschkova[6] and Macakova, Blomberg, and Claesson[9] monitored surfactant adsorption with a quartz crystal microbalance (QCM) and an optical technique in parallel but on separate substrates for each instrument. Stålgren, Erikkson, and Boschkova used null ellipsometry as the optical technique while Macakova, Blomberg, and Claesson used optical reflectometry. In their analysis, which included quantitative porosity on mass and volume bases, Macakova, Blomberg, and Claesson assumed the adsorbate thickness during their *in situ* investigations from a neutron scattering experiment and determined the index of refraction of the organic layer.[9] Richter and Brisson studied the adsorption of lipid vesicles with a quartz crystal microbalance with dissipation (QCM-D), null ellipsometry, and atomic force microscopy, separately.[8] Swann *et al*. used a dual polarization interferometry (DPI) waveguide setup to measure the thickness and conformation of protein adsorption. Aulin *et al*. used QCM-D and DPI on separate silica surfaces to study polyelectrolyte layer-by-layer adsorption. Domack *et al*. used QCM and ellipsometry on the same substrate to study polymer brush swelling. The authors observed that the thickness of the organic films, which were above the ultra-thin film limit, were twice as large measured by the QCM than that measured by ellipsometry, indicative of non-zero porosity.[5] Broch *et al*. reported on combined *in situ* spectroscopic ellipsometry (SE) and electrochemical quartz crystal microbalance (EQCM) instrumentation to monitor thickness and optical property variation of thin films formed by electrode anodization.[11]

In this contribution, we discuss our approach to quantitatively determine the *in situ* thickness *and* porosity of rigid, transparent, organic ultra-thin films by simultaneous SE and QCM measurements on the same sample. Our instrumental technique implements a virtual separation approach, which enables the determination of both porosity and physical thickness of ultra-thin films.[12] Material properties that must be known or assumed are the dry organic adsorbate index of refraction, n_o; the dry organic adsorbate density, ρ_o; the ambient index of refraction, n_a; and the ambient density, ρ_a. SE and QCM allow the simultaneous acquisition of dynamic measurements that incorporate many individual time slices of experimental data. The time resolution for the dynamic measurements may be adjusted for observation of the kinetic behavior of ultra-thin films. With a multiple-inlet fluid control system, the liquid ambient over a substrate can be exchanged to introduce adsorbate or begin a non-equilibrium process. The scope of this report is to present the overall instrumental approach and its use for monitoring multiple-layered organic ultra-thin film formation.

II. THEORY

Our objective is to obtain (a) thickness parameters and (b) porosity in the form of an adsorbate fraction parameter for a rigid, transparent, organic ultra-thin film. The thickness and adsorbate fraction parameters stem from SE and QCM measurement parameters converted from raw instrumental data. In this section, the SE and QCM techniques are described; a virtual separation approach, which demonstrates how SE is not sensitive to ambient inclusions in an ultra-thin film, is discussed; and equations that yield the thickness and adsorbate fraction parameters of an ultra-thin film are provided.

A. Spectroscopic ellipsometry

Ellipsometry measures normalized Fourier coefficients that describe the change of polarization state, commonly defined as the complex ratio ϱ, for an electromagnetic wave that reflects off or is transmitted through a sample. Input and output polarizations are described by linearly independent (e.g., p and s components) complex amplitudes of the probing electromagnetic wave, such that[13–15]

$$\varrho = \frac{\left(\frac{B_{\zeta'}}{B_{\xi'}}\right)}{\left(\frac{A_{\zeta}}{A_{\xi}}\right)} = \tan(\Psi)\exp i\Delta. \tag{1}$$

ϱ is often presented via real-valued parameters Ψ and Δ, where $\tan(\Psi)$ is the absolute value of ϱ, and Δ denotes the relative phase change of the p and s components of the electromagnetic wave.

Because the equations relating Ψ and Δ to physical sample parameters, such as layer thicknesses and optical constants, are nonlinear, a model must be made to describe the optical system. The model incorporates sample geometry, layer structure, and polarizability properties of component materials. Data analysis makes use of nonlinear regression methods, where measured and model-calculated ellipsometry spectra are matched as closely as possible by varying appropriate model parameters. The details of ellipsometry data analysis are beyond the scope of this work, and we direct interested readers to more thorough discussions in the literature.[16–18]

1. Pseudodielectric model function approach

The pseudodielectric function $\langle\varepsilon\rangle$ is a common representation of the ellipsometric data Ψ and Δ via the two-phase (ambient-substrate) model.[13,18] The pseudodielectric function eliminates the angle-of-incidence dependence from Ψ and Δ for the ideal optical ambient-substrate model situation.[19–21]

$$\langle\varepsilon\rangle = \varepsilon_a\left(\left(\frac{1-\rho}{1+\rho}\right)^2\sin^2\Psi_a + \cos^2\Psi_a\right)\tan^2\Psi_a. \tag{2}$$

The ambient dielectric function ε_a is unity for normal ambient or vacuum. The pseudodielectric function $\langle\varepsilon\rangle$ is often used to represent the dielectric function of a bulk sample whose surface is not ideally clean (covered, for example, with organic contaminants) and for electronic surface states that alter the dielectric function in the close vicinity of the surface.

For liquids, the ambient dielectric function is either measured independently using the minimum deviation technique[22] or taken from standard libraries. Typically the ambient fluid is transparent in the visible range, so the ambient dielectric function can be represented by the ambient index of refraction n_a.

2. Virtual separation approach

A virtual separation approach for arbitrarily segregating a heterogenous ultra-thin film into separate homogenous sublayers from an ellipsometric modeling point of view has been previously described.[12] The major points are summarized here. Through a 4×4 matrix modeling approach, also known as the Berreman-formalism,[13,18,23–26] a transfer matrix $\mathbf{T}$ can completely describe a linear optical system. $\mathbf{T}$ consists of an ordered product of partial transfer matrices ($\mathbf{T}_p$), which describe homogenous constituent sublayers, and matrices that describe incident (ambient, $\mathbf{L}_a$) and exit (substrate, $\mathbf{L}_f$) mediums, such that

$$\mathbf{T} = \mathbf{L}_a^{-1}\mathbf{T}_{p,1}^{-1}\ldots\mathbf{T}_{p,N}^{-1}\mathbf{L}_f. \tag{3}$$

The partial transfer and medium matrices typically do not multiplicatively commute. However, if the ultra-thin film limit is met, i.e., when $2\pi nd/\lambda \ll 1$, where n is the index of refraction and λ is the wavelength of probing light, the partial transfer matrix product of Eq. (3) can be approximated as a matrix sum. Thus, the partial transfer matrices become interchangeable. Consider a porous ultra-thin film that has an "effective" thickness d_{eff} and an effective index of refraction n_{eff}. The partial transfer matrices describing constituent ambient inclusions (d_a, n_a) may be moved via additive commutation to the top of the layer stack, forming an ambient-ambient interface and leaving the constituent adsorbate material (d_o, n_o). Linear polarization-dependent techniques, e.g., ellipsometry, are therefore not sensitive to the amount of ambient material in a porous, transparent ultra-thin film. The virtual separation approach renders the linear averaging scheme between the dielectric constants of the embedded materials as a valid effective medium consideration for the mixed-material ultra-thin layer and is different from the commonly known Bruggeman or Maxwell-Garnett effective medium approximations. The latter are derived for three-dimensional mixtures of geometrical inclusions with dimensions much smaller than the probing wavelength. The effective medium consideration changes when approaching a mixture in two dimensions, and the discussed approach in our paper presents the correct results for the effective medium mixing in that case.

3. Parameter accessibility

Formation of an ultra-thin film consisting of a mixture between adsorbate and ambient constituents is experimentally detected by parameters $\delta\Psi$ and $\delta\Delta$, which are the deviations from Ψ and Δ, respectively, that are measured prior to thin film formation. In this case, Ψ and Δ describe the bare substrate within a liquid cell filled with the fluid ambient or with a set of different thin films already present before ultra-thin film formation. $\delta\Psi$ and $\delta\Delta$ depend on the product $n_o d_o$. If n_o can be assumed, e.g., from experimental results or the literature, inversion of the ellipsometric parameters then delivers d_o, which is termed d_{SE} in this work. We define the SE measurement parameter X^{SE} as the index-thickness product,

$$X^{SE} \equiv n_o d_{SE}. \tag{4}$$

X^{SE} is acquired by constructing an optical model for the experimental system (substrate-organic adsorbate-ambient), describing the dielectric function for each optical model component, and varying X^{SE} in the optical model until experimental data and optical model-generated data best match. Without further proof, it can be shown that the variation in $\delta\Psi$ due to $n_o d_{SE}$ is much less pronounced than in $\delta\Delta$.[15] Therefore, $\delta\Delta$ bears much higher sensitivity to thin film formation and is reported commonly, for example, from real-time *in situ* measurements of organic ultra-thin film attachment.

Another result of the ultra-thin film approximation is that the index-thickness product cannot be resolved; in addition to systematic and random errors of measured $\delta\Delta$, the relative error for d_{SE} is the same as for the assumed n_o.[12,16,17]

B. Quartz crystal microbalance

A quartz crystal microbalance measures vibrational frequency changes of a quartz crystal sensor's odd harmonic resonance overtones. The quartz crystal is cut such that it vibrates in a shear mode due to the piezoelectric effect. The quartz crystal can be coated with metal to act as top and bottom electrode contacts. The sensor top contact is used as the experimental substrate.[27]

For rigid films, the correlation between a frequency shift of $\delta\nu_{N_{ov}}$, where overtone $N_{ov} = 3, 5, \ldots$, and the change in attached mass per unit area Γ_{QCM} is linear and described by the Sauerbrey equation,[28]

$$X^{QCM} \equiv \rho_{eff} d_{QCM} = \Gamma_{QCM} = -\frac{\delta\nu_{N_{ov}}\sqrt{\rho_q \mu_q}}{2\nu_0^2 N_{ov}}, \tag{5}$$

where ρ_{eff} is the average, effective density of the ultra-thin film, d_{QCM} is the total thickness of the porous ultra-thin film that includes ambient inclusions, ρ_q is the density of quartz, and μ_q is the shear modulus of quartz. We define here the QCM measurement parameter X^{QCM}, which is commonly reported as the surface density Γ_{QCM}. As explained in Sec. II A 3 for the index-thickness product, the density-thickness product $\rho_{eff} d_{QCM}$ cannot be resolved, either.

Because the Sauerbrey equation assumes a rigid film scenario, to determine film viscoelasticity a variation of QCM known as quartz crystal microbalance with dissipation (QCM-D) is used to also measure the shifts in signal dissipation of the odd harmonic overtones.[29] In a manner similar to ellipsometry data analysis, physical film parameters in a viscoelastic model that includes the Voigt constitutive equation, for example, are varied as model-generated frequency and dissipation data are best-matched to experimental results.[29] For our specific application to ultra-thin films, however, dissipation shifts are typically small, and detected viscoelastic effects do not provide sufficient sensitivity for breaking the density

-thickness product. We therefore limit our discussion to the rigid scenario.

C. Experimental parameters

Once the measurement parameters X^{SE} and X^{QCM} have been determined, they can be used with assumed or known material properties (volumetric densities and optical indices of refraction) to obtain the thickness (d_{SE} and d_{QCM}) and adsorbate fraction (f_o^m and f_o^V for mass and volume bases, respectively) parameters.

1. Determination of X^{SE}

A layered substrate-organic adsorbate-ambient optical model is used to calculate the ellipsometric response of the sample when the ultra-thin film is being formed or modified. The dielectric function of each component in the optical model must be known. The ellipsometric measurement parameter $X^{SE} \equiv n_o d_{SE}$ is obtained by variation of d_{SE} until measured and calculated SE data match as closely as possible. The first step is to measure and determine the substrate dielectric function from a clean surface. We have previously discussed changes, first described by Drude,[15] in the imaginary part of the substrate dielectric function upon introduction of liquid ambient due to contaminant removal.[30] As we cannot be certain our substrate surface is absolutely free of organic contaminants prior to ultra-thin film growth, we obtain the substrate dielectric function by determining its pseudodielectric function. The spectral dependence of the substrate pseudodielectric function is conveniently modeled via parameterization using a basis-spline (B-spline) function[31]. The remaining unknown within this model is the index of refraction of the organic ultra-thin film. Because the ultra-thin film is assumed to be transparent, we set its extinction coefficient to zero ($k_o = 0$). We further assume, without loss of generality, the index of refraction is wavelength independent, i.e., $n_o(\lambda) = n_o$.

2. Determination of fraction and thickness parameters

The quantities n_o, ρ_o, n_a, and ρ_a must be known or assumed. d_{SE} can be immediately found from the definition of X^{SE}, where

$$d_{SE} = \frac{X^{SE}}{n_o}. \tag{6}$$

For the scenario where $\rho_o = \rho_a$, the effective density ρ_{eff} of the ultra-thin film is constant. This scenario is relevant if (a) the adsorbate density is known to be very similar to the ambient density or (b) the adsorbate density cannot be determined. The second justification would apply, for example, if the adsorbate is a powder outside of solution and molecular packing phenomena prevent density measurement. Mass and volume fractions of the ultra-thin film are equivalent.

With ρ_{eff} known, the QCM thickness d_{QCM} is acquired from the definition of X^{QCM}, where

$$d_{QCM} = \frac{X^{QCM}}{\rho_{eff}}. \tag{7}$$

The adsorbate content fraction $f_o^{m,V} = f_o^m = f_o^V$ is given by

$$f_o^{m,V} = \frac{d_{SE}}{d_{QCM}}. \tag{8}$$

In the scenario of different densities for the adsorbate and ambient, ρ_{eff} may vary with time during a dynamic measurement as the porosity changes. Consequently, mass and volume fraction parameters may be different.

$$f_o^m = \frac{m_o}{m_o + m_a} = \frac{m_o}{m_{eff}}, \tag{9}$$

$$f_o^V = \frac{V_o}{V_o + V_a} = \frac{V_o}{V_{eff}}, \tag{10}$$

where m_o (V_o) is the adsorbate mass (volume), m_a (V_a) is the mass (volume) of ambient inclusions, and m_{eff} (V_{eff}) is the total ultra-thin film mass (volume).

The masses in Eq. (9) can be rewritten as density-thickness-area products to find f_o^m, such that

$$f_o^m = \frac{\rho_o d_{SE} A}{\rho_{eff} d_{QCM} A} = \frac{\rho_o d_{SE}}{\rho_{eff} d_{QCM}}. \tag{11}$$

An arbitrary area of the sample is described by A, which is simplified out of Eq. (11) because the arbitrary area is the same whether the ultra-thin film includes ambient inclusions or not. Because neither d_{QCM} nor ρ_{eff} is known at the moment, Eq. (11) is rewritten in terms of the SE and QCM measurement parameters to take the following form:

$$f_o^m = \frac{\rho_o}{n_o} \frac{X^{SE}}{X^{QCM}}. \tag{12}$$

Thus, f_o^m is obtained from a measurement if ρ_o and n_o are known or can be assumed.

We identify ρ_{eff} as the weighted average of the component densities, such that

$$\rho_{eff} = f_o^V \rho_o + \left(1 - f_o^V\right) \rho_a. \tag{13}$$

It can be shown that

$$f_o^V = \frac{\rho_{eff}}{\rho_o} f_o^m. \tag{14}$$

By combining Eqs. (13) and (14), one obtains f_o^V.

$$f_o^V = \frac{\rho_a}{\rho_o} \frac{f_o^m}{1 - f_o^m + f_o^m \frac{\rho_a}{\rho_o}}, \tag{15}$$

which allows ρ_{eff} to be found from Eq. (13). Finally, d_{QCM} is found from Eq. (7).

3. Comparison of thickness and surface density parameters

Whether to report the quantity of ultra-thin film attachment as a thickness (d) or surface density (Γ) parameter is a matter of preference. The algorithm to obtain the fraction parameters does not change significantly if surface density parameters are maintained. Note that when ρ_o or ρ_{eff} equals 1 g/ml, the respective thickness parameter in units of nm is

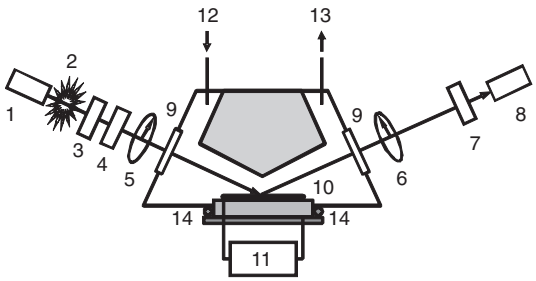

FIG. 1. Schematic diagram for experimental setup. 1—tungsten light source, 2—unpolarized light, 3—polarizer, 4—rotating compensator, 5—polarized light, 6—polarized light altered by sample surface, 7—analyzer, 8—detector, 9—optical windows, 10—QCM sensor surface, 11—QCM sensor control, 12—liquid inlet, 13—liquid outlet, and 14—O-ring for sealing.

equal in magnitude to the respective surface density parameter, $\Gamma_{\mathrm{QCM}} = \rho_{\mathrm{eff}} d_{\mathrm{QCM}}$ and $\Gamma_{\mathrm{SE}} = \rho_{\mathrm{o}} d_{\mathrm{SE}}$, in units of mg/m^2.

III. COMBINATORIAL APPROACH TO CHARACTERIZE ULTRA-THIN FILMS

A. Experimental setup

Fig. 1 illustrates the temperature-controlled liquid cell where ultra-thin films are measured. The liquid cell acts as a lid, and the QCM sensor provides the bottom seal with an O-ring. Fluid inlet and outlet ports allow for ambient liquid solution exchange, and windowed optical channels at a 65° angle of incidence from the QCM sensor normal allow the ellipsometry beam to proceed through the cell and probe the sample.

Fig. 2 shows a schematic for the entire experimental setup, including the multiple-inlet fluid control system. The nomenclature for italicized symbols that represent control parameters is given in Table I. Inlet reservoirs R_s contain fluids that can be pumped by respective inlet pumps P_s through a multiple-port valve $\mathrm{V_c}$ and a bypass valve $\mathrm{V_b}$. $\mathrm{V_b}$ allows the user to redirect flow to $\mathrm{R_d}$ and avoid the liquid cell. The fluid then proceeds through the temperature-controlled liquid cell and an optional/alternative drain pump $\mathrm{P_d}$ before removal to a drain reservoir $\mathrm{R_d}$. The pumps, valves, and liquid cell temperature are computer-controlled via user interfaces.

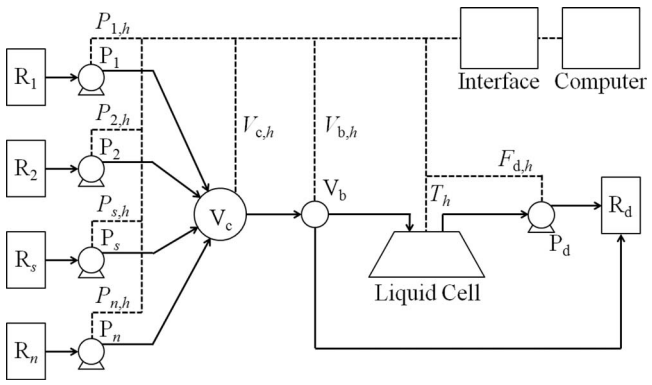

FIG. 2. Schematic of the experimental setup. Solid lines represent fluid lines and dotted lines represent an electronic logic control connection.

TABLE I. Notation for controlled experimental parameters. The inlet pumps, drain pump, multiple-port valve, bypass valve, and liquid cell temperature are controlled by parameter sets $P_{s,h}$, $P_{\mathrm{d},h}$, $V_{\mathrm{c},h}$, $V_{\mathrm{b},h}$, and T_h, respectively. Upon each measurement period τ, the next set of equipment parameters is called. $h = 0, 1, \ldots, m-1$ where m is an integer that defines the total number of data sets in a dynamic measurement.

Parameter	$t = 0$	$t = \tau$	...	$t = h\tau$
$P_{s,h}$	$P_{s,0}$	$P_{s,1}$	...	$P_{s,h}$
$P_{\mathrm{d},h}$	$P_{\mathrm{d},0}$	$P_{\mathrm{d},1}$	...	$P_{\mathrm{d},h}$
$V_{\mathrm{c},h}$	$V_{\mathrm{c},0}$	$V_{\mathrm{c},1}$	...	$V_{\mathrm{c},h}$
$V_{\mathrm{b},h}$	$V_{\mathrm{b},0}$	$V_{\mathrm{b},1}$	...	$V_{\mathrm{b},h}$
T_h	T_0	T_1	...	T_h

The SE and QCM are controlled via computer interface and acquire measurements simultaneously. Each data set that partially constitutes a dynamic measurement is taken at a particular time slice. The measurement period τ is defined as the amount of time between two consecutive data sets, and the total number of data sets in a dynamic measurement is m. τ and m are adjusted and set by the user prior to the beginning of a dynamic measurement. The time slice of a data set or control parameter is identified by the integer subscript $h = 0, 1, \ldots, m-1$.

The inlet pumps, drain pump, multiple-port valve, bypass valve, and liquid cell temperature have control parameter sets $P_{s,h}$, $P_{\mathrm{d},h}$, $V_{\mathrm{c},h}$, $V_{\mathrm{b},h}$, and T_h, respectively. At every time slice of a dynamic measurement, each parameter set has its values predefined in the user interface. For example, at time $t = h\tau$, $P_{s,h}$ may be the flow rate for the inlet pump P_s, and $V_{\mathrm{c},h}$ could be an ordered set of s on or off designations, represented by 1 or 0, respectively, to denote what inlet lines are opened or closed by the multiple-port valve $\mathrm{V_c}$.

B. Data acquisition procedures

Fig. 3 illustrates the SE/QCM data acquisition procedure. The total length of a dynamic measurement is implied by Fig. 3 as the product $m\tau$. Before the dynamic measurement, three separate SE-only data sets are taken. First, the liquid cell lid is removed, and a new quartz sensor is placed on the liquid cell bottom. The SE angle of incidence is set to the liquid cell's machined optical port angle (65°), and an SE measurement, denoted here as "SE-NoCell," is taken. Next, the liquid cell lid is attached with the quartz sensor inside. The SE angle of incidence is then adjusted so the probing light beam can proceed through the liquid cell, if necessary. SE measurement "SE-Cell" is acquired at this point. Next, the liquid cell is filled with the liquid ambient of choice, and SE measurement "SE-Liq" is then taken.

At this point, the dynamic measurement is ready to begin, and τ and m are set. To start the dynamic measurement, SE and QCM data sets "SE-Dyn$_0$" and "QCM-Dyn$_0$," respectively, are taken while initial ($h = 0$) flow parameters are in effect. At the hth period of τ time in the dynamic measurement, the current SE and QCM data sets are SE-Dyn$_h$ and QCM-Dyn$_h$, respectively. If the preset flow parameters change at the hth period, the controlled flow units are updated. The

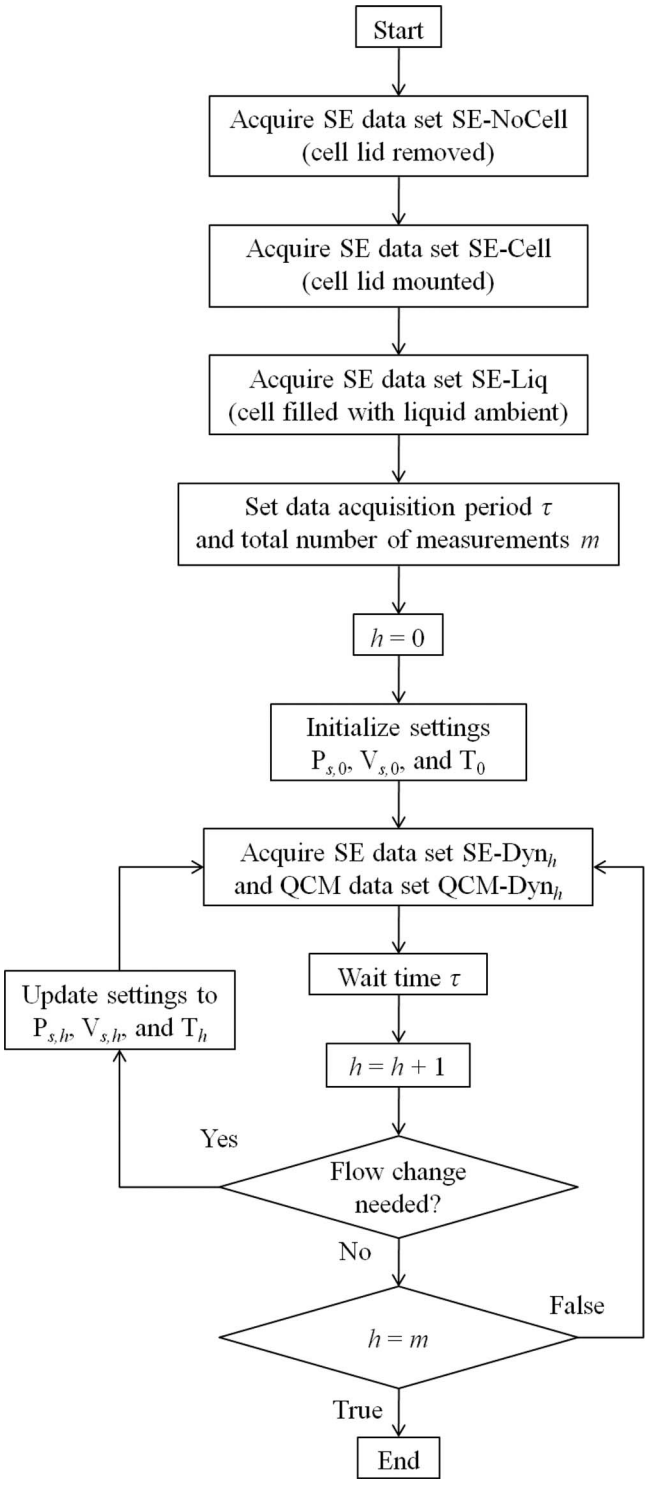

FIG. 3. Data acquisition flowchart.

final data set is recorded at time slice $m - 1$ and the dynamic measurement ends one period of τ time later.

C. Data analysis procedures

The raw SE and QCM data are analyzed through the protocol summarized by Fig. 4. The optical model described in Sec. II can now be built by incorporating the three separate SE data sets. Substrate B-spline function parameters, offsets due to window and angle-of-incidence effects, and substrate modification due to liquid rinsing are accounted for by best-matching SE-NoCell, SE-Cell, and SE-Liq data, respectively, to data generated by the optical model. The index-thickness product X^{SE} that describes the adsorbate component of the organic ultra-thin film is then added to the optical model. X^{SE} is varied with best-matching for every time slice in the dynamic SE data set SE-Dyn$_h$.

d_{SE} is found for each time slice of SE-Dyn$_h$ by Eq. (6), assuming n_o. Next, Eq. (5) is used to find X^{QCM} from QCM-Dyn$_h$.

If identical ρ_o and ρ_a are assumed (Scenario 1 from Sec. II C 2), we have $\rho_{eff} = \rho_o = \rho_a$, and Eq. (7) is used to find d_{QCM}. The adsorbate fraction parameter for both mass and volume can then be found for each time slice of data via Eq. (8).

If ρ_o and ρ_a are different (Scenario 2 from Sec. II C 2), Eq. (12) is used to find f_o^m. f_o^V can then be found from Eq. (15). Then ρ_{eff} for each time slice is found from Eq. (13). Finally, d_{QCM} is calculated from Eq. (7).

IV. EXPERIMENTAL APPARATUSES

A commercially available liquid cell equipped with a QCM-D apparatus (Q-Sense E1 SE/QCM-D Module, Biolin Scientific) and optical access windows was set up with a spectroscopic ellipsometer (M-2000-UV, J.A. Woollam Co.). The liquid cell was designed to promote optimal flow effects, avoid disruption via air bubbles, and use a low volume to conserve fluid (Fig. 1). The ellipsometer measures 512 wavelengths simultaneously in the spectral region from 370 to 1000 nm. The windows in the liquid cell allow for optical access for SE measurements at a 65° angle of incidence. The liquid cell is equipped with temperature control and air-sealed inlet and outlet lines for the introduction and exchange of solutions. The bottom of the liquid cell is connected to the QCM-D instrumentation. The software, CompleteEASE® (J.A. Woollam Co.) and QSoft™(Biolin Scientific), control the M-2000-UV and E1 QCM-D data acquisition, respectively, and QSoft also controls the temperature of the liquid cell. Control of liquid flow, rate, and times can be achieved with a high-performance liquid chromatography (HPLC) system, such as the Agilent 1200 Infinity LC.

V. CASE STUDIES

A. Surfactant adsorption

Cetyltrimethylammonium bromide (CTAB) is a cationic surfactant with a nonpolar hydrocarbon "tail" and an ammonium salt "head" group. At ~1 mM, the critical micelle concentration (CMC), full micelles are formed in aqueous CTAB solutions, where the nonpolar tails are shielded by the polar head groups.[32] Surfactants like CTAB are useful for nanoparticle synthesis[33] and detergent applications.[34] We have previously studied the adsorption of CTAB from solutions above the CMC onto gold with SE/QCM,[30] and in this contribution we detail SE/QCM measurement of the adsorption process from solutions below the CMC. 0.1 mM CTAB

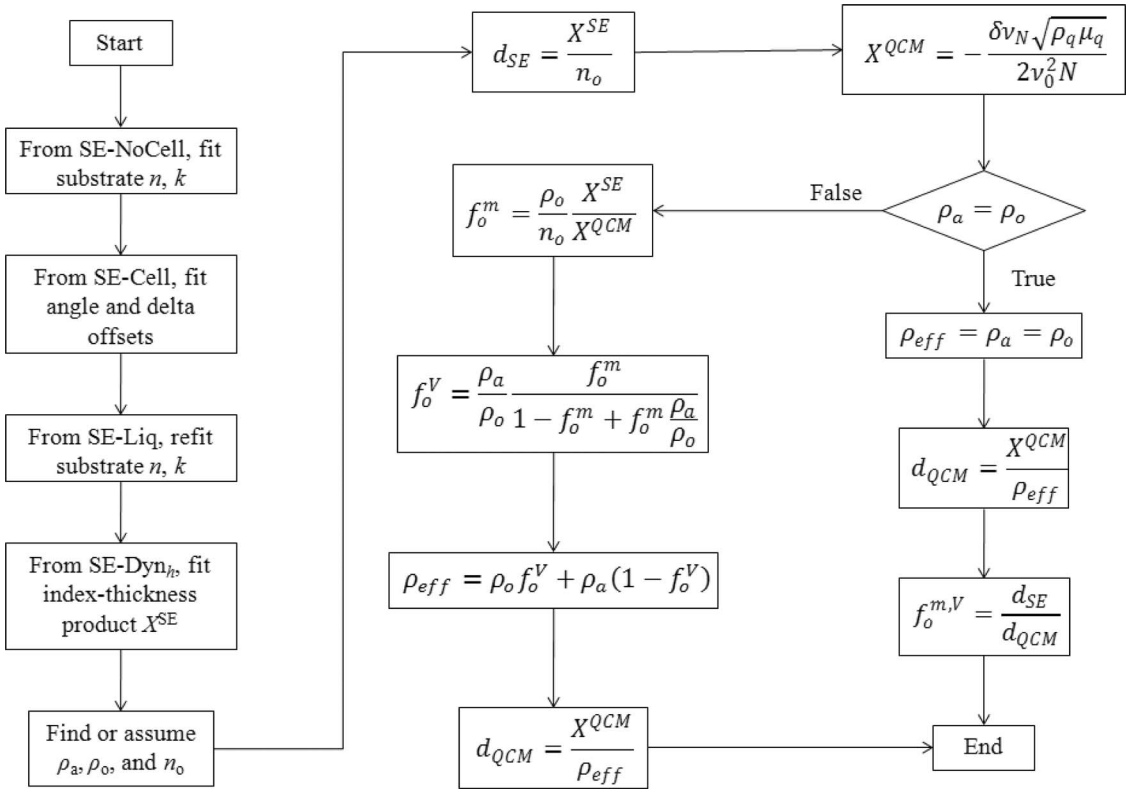

FIG. 4. Data analysis flowchart.

aqueous solution was made with no additives. The CTAB was purchased from Sigma-Aldrich, and 18.2 MΩ-cm water was prepared from a Barnstead Nanopure water purification system. Water was introduced from its respective reservoir (R_1) through the liquid cell at 0.4 ml/min to achieve a stable baseline. Next, V_c was turned to switch the reservoir to that containing the 0.1 mM solution of CTAB (R_2). After ~10 min of CTAB solution flow, V_c was reversed, and ~10 min of water flow (rinse) was allowed before the experiment ended. For data analysis, n_o was assumed to be 1.5, and ρ_a is ~1 g/ml. The value of ρ_o was not readily known, as dry CTAB is a solid at standard conditions, and effects including packing density must be considered. We elected to simply set ρ_o to 1 g/ml. As a result, the first scenario of data analysis in Fig. 4 was used to derive the thickness and adsorbate fraction parameters.

Figure 5 shows the results of CTAB adsorption onto gold from a 0.1 mM aqueous solution. At ~$t = 11$ min, the CTAB solution entered the liquid cell, and at $t = 20$ min, purified water was pumped through the liquid cell. The adsorption and desorption processes are both simple, and $f_o^{m,V}$ is fairly uniform throughout attachment and rinsing. This observation indicates that the CTAB molecules assemble in flat patches with uniform density within the patches, where growth or rinsing occurs by adding or removing molecules at the boundaries of the patches. The slight decrease of the adsorbate fraction during rinsing could be attributed to water displacing individual CTAB molecules within the still cohesive film patches. Similar measurements can be used to determine adsorption isotherms.[35]

B. Self-assembled monolayer chemisorption

Alkanethiol self-assembled monolayers (SAMs) are hydrocarbons with a sulfur head group, a hydrocarbon chain body, and a functionalized tail group that exhibits a desired surface chemistry. The sulfur head group binds to the substrate via chemisorption.[36] SAMs are useful as

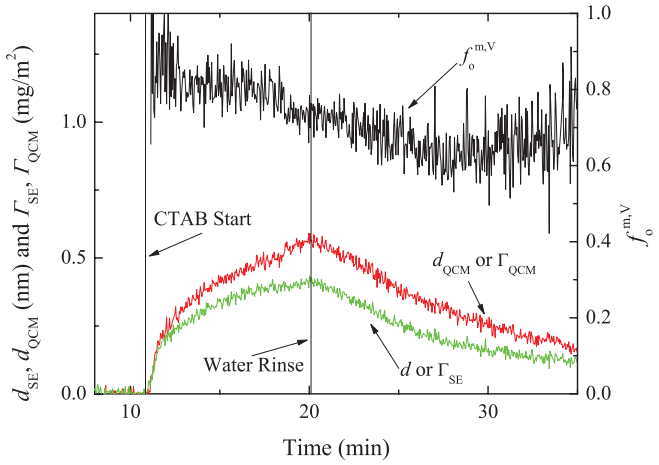

FIG. 5. (Color online) Thickness, surface density, and adsorbate fraction parameter plots of 0.1 mM CTAB solution experiment reported from SE and QCM measurements. Because (a) $f_o^{m,V}$ is relatively uniform and (b) the thickness parameters change monotonically over the adsorption and desorption processes, it can be inferred that the CTAB ultra-thin film was established and rinsed in a patch-wise manner. Note that because $\rho_o = \rho_a = \rho_{eff} = 1$ g/ml, the magnitudes of d in units of nm and Γ in units of mg/m^2 are identical.

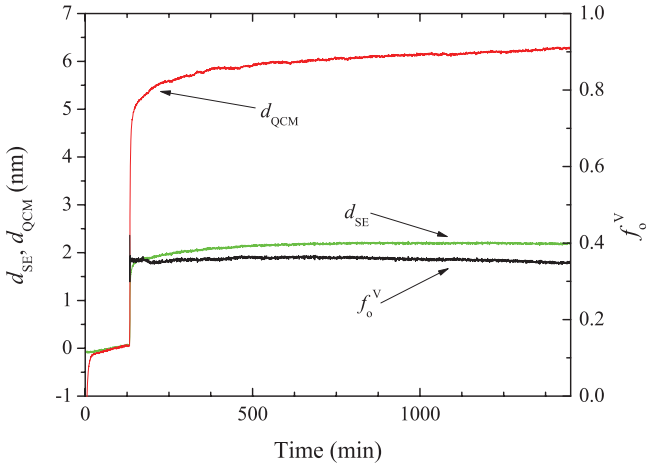

FIG. 6. (Color online) Thickness and adsorbate fraction plots of 2 mM 8-mercapto-1-octanol solution experiment reported by SE and QCM. A fast initial growth step is followed by a slower second process, and the porosity represented by the adsorbate fraction parameter is consistent throughout chemisorption.

uniform, cost-effective coatings for adjusting a substrate's surface properties.[36] We have shown 1-decanethiol chemisorption onto gold from an ethanol solution as monitored by SE/QCM.[37] Here we demonstrate a similar scenario, but of 8-mercapto-1-octanol in an aqueous solution.

8-mercapto-1-octanol was purchased from Sigma-Aldrich and used to prepare a 2 mM solution in purified water with no additives. Pure water and alkanethiol solution had separate reservoirs and pumps that pushed the solutions at 0.1 ml/min through V_c, V_b, and the liquid cell to R_d. At $t = 100$ min, the inlet fluid was switched from water to alkanethiol solution. After ~100 min, the alkanethiol pump was turned off, and the solution over the quartz sensor became stagnant as the measurement continued overnight.

For this system we used measured values of $n_o = 1.484$ and $\rho_o = 0.93$ g/ml (Sigma-Aldrich). Therefore, the $\rho_o \neq \rho_a$ scenario was used for analyzing the SAM chemisorption data.

The results for the SAM chemisorption experiment are shown in Fig. 6. At $t = 150$ min, two distinct stages in the SAM chemisorption process are evident, in agreement with the literature.[36] f_o^V is uniform throughout the measurement, implying that the porosity is consistent throughout the ultra-thin film growth. The combinatorial SE/QCM technique thus provides a quantitative measure of the ultra-thin film porosity.

C. Selective DNA detection

SAMs that incorporate single-stranded DNA molecules are widely used for analytical applications that include genotyping,[38] protein and small molecule detection,[39,40] and high-throughput affinity screening.[41] Characterizing the formation and interrogation of DNA-based sensors using SE/QCM has the potential to elucidate factors that contribute to sensor response, such as surface conformation and hybridization efficiency. The probe sequence used here is a well-characterized genosensor specific for a region surrounding codon 12 of the *K-ras* gene, mutations of which are often present in pancreatic cancer lesions.[42]

The DNA probe was conjugated to a six-carbon alkanethiol moiety for attachment to a gold substrate and subsequently embedded with a SAM of 6-mercapto-1-hexanol to enhance stability. We demonstrate that SE/QCM is capable of characterizing sub-nanometer average thickness changes and the porosity of multiple-component, biological, ultra-thin films.

To study the utility of SE/QCM in the characterization of bioactive films, DNA sensors were fabricated and interrogated *in situ*. The running buffer (20 mM Tris, 140 mM NaCl, 5 mM KCl, 1 mM $CaCl_2$, 1 mM $MgCl_2$, pH 7.4, filtered with a 0.2 μm syringe filter immediately before use) was used to make all solutions and was exchanged into the liquid cell as a rinse between each step of sensor fabrication and interrogation. *K-ras* stem-loop DNA probe and BRCA2 and *K-ras* targets were purchased from Biosearch Technologies (Novato, CA). All salts, Tris buffer, and 6-mercapto-1-hexanol were purchased from Sigma-Aldrich. Tris(2-carboxyethyl)phosphine was purchased from Soltec Ventures (Beverly, MA). A flow rate of 50 μL/min was used throughout the experiment. Here we assumed $n_o = 1.5$ and $\rho_o = 1$ g/ml. General values were chosen to reflect the variety of organic materials that composed the ultra-thin film.

Fig. 7 presents changes in thickness and porosity associated with probe chemisorption,[43] 2 mM 1-mercapto-6-hexanol SAM formation, and interrogation with non-complementary[44] and complementary[45] DNA fragments.

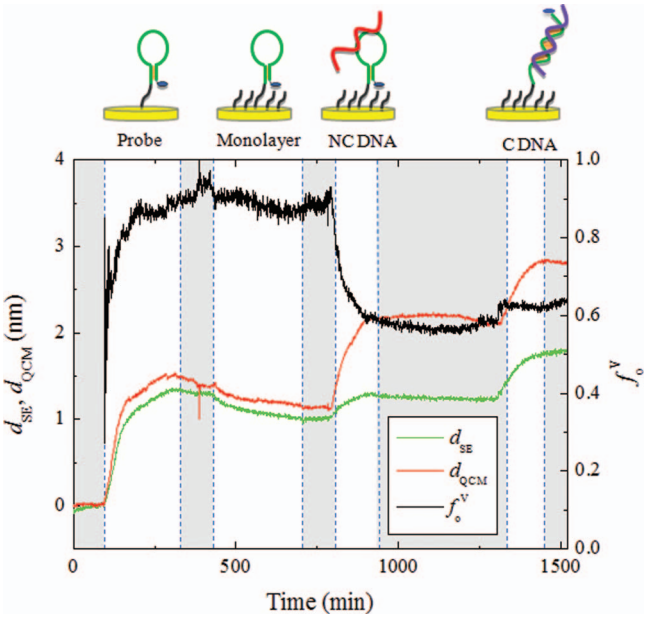

FIG. 7. (Color online) Thickness and adsorbate fraction plots of a multiple-component organic film. Insertions of probe aptamer, SAM, non-complementary DNA, and complementary DNA are denoted by Probe, Monolayer, NC DNA, and C DNA, respectively. Note the decrease in thickness upon SAM chemisorption, the shifts in adsorbate fraction when non-complementary and complementary DNA are introduced, and the differences between SE and QCM responses for non-complementary and complementary DNA interrogation.

d_{SE} reflects the dry thickness of the multiple-component layer and does not distinguish between constituent adsorbate materials. d_{QCM} includes d_{SE} and ambient inclusions. The thickness parameters for the multiple-component layer remain below the ultra-thin film limit. During probe chemisorption, we observe the formation of a well-packed DNA layer, as evidenced by the similarity of the thickness change reported in SE and QCM. The adsorbate volumetric fraction remains high upon the introduction of the passivating SAM. Interestingly, d_{SE} decreases during SAM formation, suggesting that large DNA probes are displaced by relatively short SAM molecules. Interrogation with a non-specific strand of DNA yielded a response in both the SE and the QCM detectors. The discrepancy between the two responses, however, indicates the non-specific DNA formed a porous layer on the surface. The non-complementary DNA results contrast sharply with our observation of nearly identical SE and QCM responses upon the introduction of the complementary *K-ras* segment of equal length and implies the existence of distinct mechanisms for specific and non-specific binding.

VI. SUMMARY

In conclusion, we described a combinatorial SE/QCM technique for monitoring the real-time thickness and porosity evolution of rigid, transparent, organic ultra-thin films. The hybrid approach is necessary because neither optical SE nor acoustical QCM can independently distinguish between the thickness and porosity of films that meet the ultra-thin film limit $2\pi nd/\lambda \ll 1$. Using a virtual separation approach, we were able to arbitrarily rearrange the components of heterogeneous, isotropic ultra-thin films from the standpoint of SE. Equations for determining an ultra-thin film's thickness and adsorbate fraction parameters from SE and QCM raw data were derived. We considered different scenarios of the measured system whereby the dry adsorbate and liquid ambient densities were equal or not. Data acquisition protocols for use with a multiple-flow inlet control system were introduced. Finally, we discussed the application of SE/QCM toward analyzing relevant single- and multiple-layer organic ultra-thin films.

ACKNOWLEDGMENTS

The authors gratefully acknowledge support from The Procter & Gamble Company, The J.A. Woollam Company, Inc., Agilent Technologies, the National Science Foundation under Award No. EPS-1004094, and the University of Nebraska-Lincoln College of Engineering. They also acknowledge rewarding discussions with Matthew Wagner (The Procter & Gamble Company), Fredrik Höök (Chalmers University), and Hans Arwin (Linköping University).

[1] Q. Zhang and V. Subramanian, Biosens. Bioelectron. **22**(12), 3182 (2007).
[2] S. Sarkar, B. C. Isenberg, E. Hodis, J. B. Leach, T. A. Desai, and J. Y. Wong, J. Biomater. Sci., Polym. Ed. **19**(10), 1347 (2008).
[3] S. C. Howell, R. Mittal, L. J. Huang, B. Travis, R. M. Breyer, and C. R. Sanders, Biochemistry **49**(44), 9572 (2010).
[4] E. Bittrich, K. B. Rodenhausen, K.-J. Eichhorn, T. Hofmann, M. Schubert, M. Stamm, and P. Uhlmann, Biointerphases **5**(159), 1 (2010).
[5] A. Domack, O. Prucker, J. Rühe, and D. Johannsmann, Phys. Rev. E **56**(1), 680 (1997).
[6] J. J. R. Stålgren, J. Eriksson, and K. Boschkova, J. Colloid Interface Sci. **253**(1), 190 (2002).
[7] M. J. Swann, L. L. Peel, S. Carrington, and N. J. Freeman, Anal. Biochem. **329**(2), 190 (2004).
[8] R. P. Richter and A. R. Brisson, Biophys. J. **88**(5), 3422 (2005).
[9] L. Macakova, E. Blomberg, and P. M. Claesson, Langmuir **23**(24), 12436 (2007).
[10] C. Aulin, I. Varga, P. M. Claesson, L. Wagberg, and T. Lindstrom, Langmuir **24**(6), 2509 (2008).
[11] L. Broch, L. Johann, N. Stein, A. Zimmer, and R. Beck, Rev. Sci. Instrum. **78**(6), 064101 (2007).
[12] K. B. Rodenhausen and M. Schubert, Thin Solid Films **519**, 2772 (2011).
[13] R. M. Azzam and N. M. Bashara, *Ellipsometry and Polarized Light* (North-Holland, Amsterdam, 1984).
[14] *Handbook of Ellipsometry*, edited by H. G. Tompkins and E. A. Irene (William Andrew, Highland Mills, 2004).
[15] P. Drude, Ann. Phys. **34**, 270 (1888).
[16] G. E. Jellison, Thin Solid Films **313–314**, 33 (1998).
[17] G. E. Jellison, "Data analysis for spectroscopic ellipsometry," in *Handbook of Ellipsometry*, edited by E. A. Irene and H. W. Tompkins (William Andrew, Norwich, NY, 2004).
[18] H. Fujiwara, *Spectroscopic Ellipsometry* (Wiley, New York, 2007).
[19] D. E. Aspnes and A. A. Studna, Phys. Rev. B **27**(2), 985 (1983).
[20] D. E. Aspnes, "The accurate determination of optical properties by ellipsometry," in *Handbook of Optical Constants of Solids*, edited by E. D. Palik (Academic, New York, 1998), Vol. I, p. 89.
[21] A. Röseler, *Infrared Spectroscopic Ellipsometry* (Akademie-Verlag, Berlin, 1990).
[22] T. Berlind, G. K. Pribil, D. Thompson, J. A. Woollam, and H. Arwin, Phys. Status Solidi C **5**(5), 1249 (2008).
[23] I. Abdulhalim, L. Benguigui, and R. Weil, J. Phys. (Paris) **46**, 815 (1985).
[24] M. Schubert, "Theory and application of generalized ellipsometry," in *Introduction to Complex Mediums for Optics and Electromagnetics*, edited by W. S. Weiglhofer and A. Lakhtakia (SPIE, Bellingham, WA, 2004), pp. 677–710.
[25] M. Schubert, Phys. Rev. B **53**(8) 4265 (1996) .
[26] M. Schubert, *Infrared Ellipsometry on Semiconductor Layer Structures: Phonons, Plasmons and Polaritons*, Springer Tracts in Modern Physics Vol. 209 (Springer, Berlin, 2004).
[27] F. Höök, M. Rodahl, P. Brzezinski, and B. Kasemo, Langmuir **14**(4), 729 (1998).
[28] G. Sauerbrey, Z. Phys. A: Hadrons Nucl. **155**(2), 206 (1959).
[29] M. Rodahl, F. Höök, C. Fredriksson, C. A. Keller, A. Krozer, P. Brzezinski, M. Voinova, and B. Kasemo, Faraday Discuss. **107**, 229 (1997).
[30] K. B. Rodenhausen, M. Guericke, A. Sarkar, T. Hofmann, N. Ianno, M. Schubert, T. E. Tiwald, M. Solinsky, and M. Wagner, Thin Solid Films **519**, 2821 (2011).
[31] B. Johs and J. S. Hale, Phys. Status Solidi A **205**(4), 715 (2008).
[32] L. Sepulveda and J. Cortes, J. Phys. Chem. **89**(24), 5322 (1985).
[33] G. Wei, L. Wang, H. Zhou, Z. Liu, Y. Song, and Z. Li, Appl. Surf. Sci. **252**(5), 1189 (2005).
[34] F. van Ruissen, M. Le, J. M. Carroll, P. G. M. van der Valk, and J. Schalkwijk, J. Invest. Dermatol. **110**(4), 358 (1998).
[35] R. A. May, D. W. Flaherty, C. B. Mullins, and K. J. Stevenson, J. Phys. Chem. Lett. **1**(8), 1264 (2010).
[36] J. C. Love, L. A. Estroff, J. K. Kriebel, R. G. Nuzzo, and G. M. Whitesides, Chem. Rev. **105**(4), 1103 (2005).
[37] K. B. Rodenhausen, B. A. Duensing, T. Kasputis, A. K. Pannier, T. Hofmann, M. Schubert, T. E. Tiwald, M. Solinsky, and M. Wagner, Thin Solid Films **519**, 2817 (2011).
[38] C. Fan, K. W. Plaxco, and A. J. Heeger, Proc. Natl. Acad. Sci. U.S.A. **100**(16), 9134 (2003).
[39] X. Zuo, S. Song, J. Zhang, D. Pan, L. Wang, and C. Fan, J. Am. Chem. Soc. **129**(5), 1042 (2007).
[40] C. A. Savran, S. M. Knudsen, A. D. Ellington, and S. R. Manalis, Anal. Chem. **76**(11), 3194 (2004).
[41] J. S. Shumaker-Parry, R. Aebersold, and C. T. Campbell, Anal. Chem. **76**(7), 2071 (2004).

[42]W. Yang, J. Y. Gerasimov, and R. Y. Lai, Chem. Commun. **2009**, 2902.
[43]0.33 μM HS-$(CH_2)_6$-5′-CCGTTACGCCACCAGCTCCAAACGG-3′-$(CH_2)_7$-NH-MB. Since the probe was purchased as a disulfide with 1-mercapto-6-hexanol, 200 μM stock probe solution was treated with tris(2-carboxyethyl)phosphine for 1 hr to reduce disulfide bonds.
[44]1 μM 17-base BRCA2 gene segment (5′-TGTACTTCAGGGCCGTA-3′).
[45]1 μM 17-base *K-ras* gene segment (5′-TTGGAGCTGGTGGCGTA-3′).